City and Environment Interactions 31 (2026) 100415

Contents lists available at ScienceDirect

City and Environment Interactions

journal homepage: www.sciencedirect.com/journal/city-and-environment-interactions

Mapping heat-related risk in three mid-sized European cities

Pascal Schlechtweg [a,b,*], Alexander Brenning [a], Jukka Käyhkö [b], Lucian Sfîcă [c]

[a] Department of Geography, Friedrich Schiller University Jena, Leutragraben 1, 07743 Jena, Germany
[b] Department of Geography and Geology, University of Turku, Turku 20014, Finland
[c] Alexandru Ioan Cuza University, Faculty of Geography and Geology, Department of Geography, 20 A Carol I Street, 700506 Iaşi, Romania

ARTICLE INFO

Keywords:
Urban heat risk
Diurnal variation
Heat vulnerability
Apartment rent
Socioeconomic disparities
Environmental inequality

ABSTRACT

Urban heat risk arises from the interaction of thermal hazard, population distribution, and socioeconomic conditions, yet comparative high-resolution assessments across European cities remain limited. We develop a harmonised 100 m heat-risk framework for three climatically contrasting mid-sized cities, Iași (Romania), Jena (Germany), and Turku (Finland), using ten years of observation-based daytime and nighttime air-temperature data. The framework distinguishes societal heat risk, which reflects the number of residents exposed, from per-capita heat risk, which normalises exposure to reveal inequalities that aggregated metrics may conceal. To our knowledge, this is the first study to provide an integrated heat-risk assessment of this kind for each of the three cities, combining diurnally resolved hazard, exposure, and rent-based vulnerability at high spatial resolution.

As a fine-scale and timely proxy for vulnerability, we incorporate apartment rent from geolocated real-estate listings; while not a comprehensive socioeconomic indicator, it captures affordability- and housing-related conditions relevant to heat sensitivity. To characterise environmental context, we quantify local (100 m) and neighbourhood-scale (300 m) land-cover fractions (tree cover, impervious surfaces, grassland) and assess their statistical associations with hazard, exposure, vulnerability, and risk components using Spearman correlations. In addition, we use Lorenz curves and Gini coefficients to quantify spatial inequalities in heat risk and green infrastructure within each city.

Across all cities, societal heat risk closely follows the residential population distribution, whereas per-capita risk aligns more strongly with spatial patterns of thermal hazard and adaptive capacity. Nighttime conditions (Tropical Nights) emerge as particularly influential for both risk measures, underscoring the importance of nocturnal heat for recovery and health. Green land cover exhibits predominantly negative, and impervious surfaces predominantly positive, associations with hazard and risk, with effect sizes varying across cities and spatial scales; these relationships are interpreted as correlational rather than causal. Lorenz and Gini analyses further show that societal heat risk and green infrastructure are unevenly distributed, with pronounced inequalities in exposure and nighttime hazard, particularly in Iași and Turku.

Overall, societal heat risk is primarily governed by where people live, while per-capita risk reveals how hazard and adaptive capacity shape the burden experienced by individuals. Apartment rent offers a practical, location-specific proxy for vulnerability that can be applied where detailed socioeconomic data are limited. The proposed framework provides a transferable basis for identifying both areas where many residents are exposed and areas where individuals may face disproportionate heat burdens, supporting more context-sensitive and equitable urban heat-adaptation planning.

1. Introduction

Heat is among the most lethal weather hazards in Europe, and both the frequency and intensity of hot extremes are increasing under anthropogenic climate change [1–5]. Urban areas further amplify this burden through the urban heat island (UHI), as built materials, morphology and anthropogenic heat raise temperatures above surrounding rural areas [6,7]. With ongoing urbanization, a growing share of Europeans will experience hazardous thermal conditions during summer in their residential environments [4,8].

* Corresponding author at: Postal address: Department of Geography, Friedrich Schiller University Jena, Leutragraben 1, 07743 Jena, Germany.
E-mail addresses: pascal.schlechtweg@uni-jena.de, pascal.p.schlechtweg@utu.fi (P. Schlechtweg).

https://doi.org/10.1016/j.cacint.2026.100415
Received 15 July 2025; Received in revised form 3 June 2026; Accepted 16 June 2026
Available online 17 June 2026

Urban heat risk arises from the interaction of hazard (thermal conditions), exposure (population distribution) and vulnerability (susceptibility and adaptive capacity) [9]. Importantly, heat hazard is temporally dynamic: daytime and nighttime heat pose distinct mechanisms and health implications [10–13]. Daytime heat is dominated by outdoor exposure and radiative loads, whereas nighttime heat impedes physiological recovery and affects individuals primarily in their homes [14–19]. Despite these differences, many risk assessments still aggregate across the diurnal cycle, potentially obscuring when and where interventions should differ between daytime (e.g., shade, evapotranspiration) and nighttime (e.g., ventilation, building fabric) conditions [20–23].

Although our analysis uses outdoor air temperature, indoor conditions represent the dominant exposure setting in Europe, where people spend ~80–90% of their time indoors [24,25]. Indoor temperatures typically track and can exceed outdoor values, especially at night, depending on building characteristics such as insulation, ventilation and thermal mass [16,26–30]. We therefore interpret outdoor metrics as proxies for potential indoor stress while acknowledging that building-specific decoupling may occur.

Vulnerability to heat is shaped by socio-spatial inequalities. Housing conditions, location, affordability, and interior and exterior characteristics, strongly influence both the intensity of heat exposure and the ability to cope with it [31–35]. Access to green and blue space, an important moderator of outdoor heat, is unevenly distributed: neighbourhoods with higher imperviousness, lower tree cover and limited cooling resources often coincide with lower socioeconomic status (SES) [36–40]. This persists despite planning recommendations that all residents should live within approximately 300 m of green space [41–44]. As a result, socioeconomically disadvantaged or low-rent households face elevated risks of heat-related discomfort, illness or mortality [45–52], and young low-income renters – such as students or early-career workers - may be particularly vulnerable due to limited adaptive capacity and restricted agency to modify their housing conditions [53].

A major barrier for fine-scale risk mapping in Europe is the limited availability of high-resolution socioeconomic data as an indicator of vulnerability. Official indicators are typically not accessible at micro-scale, outdated or simply unavailable across countries. To address this gap, we use geolocated apartment rents as a pragmatic, spatially detailed proxy for vulnerability at 100 m resolution. While rent is not conceptually new in vulnerability research, previous applications have primarily focused on the United States [54–56] or China [57–60], and operate at administrative scales or using land-surface temperature rather than air temperature.

Existing European evidence shows that only a small number of studies directly integrate housing-market indicators, such as rents, sales prices, or price-to-income ratios, into analyses related to heat [61–63]. However, these studies primarily investigate how temperature or extreme heat affects housing markets, for example through changes in property values, rental prices, search intensity, transaction volumes, or affordability ratios. Recent work from Spain and Italy demonstrates that hotter days can depress housing prices and reduce market activity, while global analyses link climate hazards to shifts in housing affordability. Crucially, these contributions use housing-market metrics to measure market responses to heat, not as indicators of socioeconomic vulnerability or spatial heat risk.

Most European heat-risk studies instead rely on socioeconomic proxies, such as, deprivation indices or personal data, to characterise vulnerability [64,65], meaning that the potential of housing-market data to capture both neighbourhood-scale exposure conditions (via links to green infrastructure and urban form) and household vulnerability (via rent burden and affordability constraints) remains largely unexploited. The present study therefore differs conceptually and methodologically from prior work by using fine-scale rent data directly as a spatial proxy for vulnerability within a harmonised, multi-city heat-risk framework.

Here, we conduct a comparative, high-resolution assessment across three mid-sized European cities with distinct climatic, morphological and socioeconomic contexts – Iași (Romania), Jena (Germany) and Turku (Finland) - to examine how relationships between heat hazard, land cover and vulnerability vary across urban environments. For each of the three cities, this work represents the first integrated heat-risk assessment at such spatial resolution and conceptual depth - linking diurnally resolved hazard, exposure, and rent-based vulnerability. Further to our knowledge, no European study (i) employs apartment rent as a standalone proxy for vulnerability at ≤100 m resolution, (ii) applies this approach consistently across climatically and socioeconomically diverse cities, or (iii) combines such a proxy with harmonised observation-based daytime and nighttime air-temperature metrics.

To achieve this, we (i) derive 10 years of observation-based air-temperature fields and construct daytime (temperature days) and nighttime (tropical nights) hazard metrics at 100 m resolution; (ii) map exposure using residential population grids; (iii) operationalize vulnerability using apartment rent; and (iv) compute societal and per-capita risk. We then relate hazard and risk components to land-cover variables to quantify their statistical associations with green and built infrastructure.

2. Study area

Iași is a major city in north-eastern Romania with over 400,000 inhabitants. It is situated mainly on the lower terraces of the Bahlui River (40–80 m a.s.l.), with urban development extending onto surrounding hills up to about 400 m, creating pronounced elevation gradients and locally distinct microclimates. Summer temperatures are the highest among the three study cities (Fig. 1): mean values reach around 21–23 °C in June–August and remain above 17 °C in September, with typical midsummer maxima of 25–28 °C and nighttime minima of 15–18 °C. The dense urban core limited green space and extensive impervious surfaces contribute to a marked urban heat island (UHI), especially in central lowland areas. Although six artificial lakes and the Bahlui River provide some cooling, their influence is spatially limited.

Multiple studies using both satellite-based land-surface temperature and in situ air-temperature observations document strong intra-urban thermal contrasts in Iași, with surface UHI intensities exceeding 5 °C during heat-prone periods and restricted air dispersion that can aggravate air pollution under stable conditions [66–68].

Iași was selected to represent Eastern European urban conditions characterized by rapid urbanization, socioeconomic disparities and often insufficient adaptation infrastructure. As one of Romania's main urban centres, it combines high population density with relatively low green-space availability and social inequality, making it a relevant case for studying heat vulnerability in a post-socialist context.

Jena, located in central Germany, is a medium-sized city of about 110,000 inhabitants in the Saale valley at roughly 143 m a.s.l. The corridor-shaped valley topography moderates the local climate relative to the surrounding uplands but also limits air exchange and can promote heat accumulation.

Climatologically, Jena experiences warm but moderate summers (Fig. 1): mean temperatures are about 16.6 °C in June, 18.7 °C in July, 18.3 °C in August and 14.4 °C in September, with daytime maxima around 21–23 °C and nighttime minima of roughly 11–14 °C. On average, there are 54 summer days (Tmax ≥25 °C) and 13 hot days (Tmax ≥30 °C) per year [69], and mean annual temperature has increased by about 1.2 K since 1901–1930. Jena was selected as a representative example of a Central European, medium-sized city with marked topographic constraints and well-documented urban heat island dynamics [70], with average intensities around 1 K and peak differences of 4–7 K during calm, anticyclonic nights [71].

The combination of pronounced valley morphology, historical urban structure and ongoing expansion makes Jena a representative Central

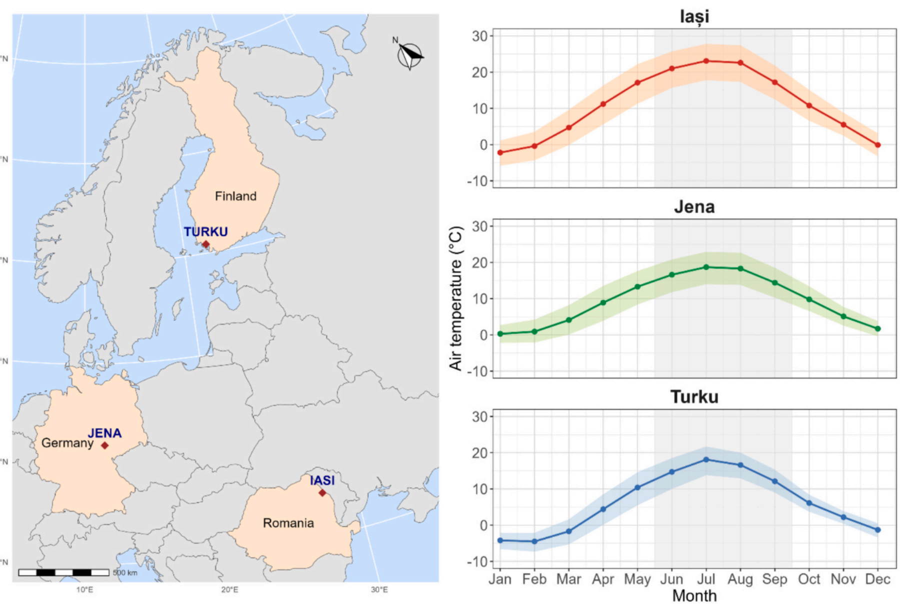

Fig. 1. (Left) Location of the three study cities Iași (Romania), Jena (Germany) and Turku (Finland) in Europe. The cities locations are highlighted as diamond markers. The map is displayed in the equal-area ETRS89 / LAEA Europe projection (EPSG:3035). Country outlines are based on Natural Earth data. (right) Monthly climatology (1991–2021) of minimum, mean, and maximum air temperature for Iași, Jena, and Turku. Ribbons show the monthly temperature range (min–max), with solid lines indicating monthly means. The summer months used in this study (June–September) are highlighted.

European case for examining intra-urban heat-risk disparities under a moderate but warming climate.

Turku is a coastal city in south-western Finland with approximately 182,000 residents. Situated at the mouth of the Aura River and embedded in a fragmented coastline and archipelago, it exhibits both maritime and inland climatic characteristics.

Despite its northern location, Turku experiences comparatively mild to warm summers (Fig. 1): mean temperatures are about 14.7 °C in June, 18.1 °C in July, 16.6 °C in August and 12.1 °C in September (1991–2021), with typical midsummer maxima of 18–22 °C and nighttime minima of 10–14 °C.

Turku shows moderate UHI effects, with mean intensities of 1–2 °C and elevated nighttime temperatures particularly in densely built-up inland neighbourhoods [72]. The city centre is on average around 2 °C warmer than the rural surroundings, and UHI intensities can occasionally reach up to 10 °C. Urban land use has been identified as the primary driver of spatial temperature variation, while topography generally plays a minor role except during nocturnal cold-air drainage or temperature inversions [73].

In the broader Finnish context, time-series analyses and climate projections indicate that warm spells and tropical nights are becoming more frequent in southern Finland, including Turku, accompanied by rising heat-related hospitalisations and fatalities [74–76].

Although Finland is often associated with cold climates, recent climatological and epidemiological studies show that Nordic populations are particularly vulnerable to heat due to limited physiological acclimatization, specific housing characteristics and rapidly increasing temperatures [18,77–79]. Even moderate heatwaves and elevated summer temperatures have been linked to indoor overheating and increased mortality and hospital admissions [18,30,74,75,77,78,80–84]. These developments underline the relevance of analysing urban heat risk in Turku alongside the Central and Eastern European cases.

3. Data and methods

3.1. Data

3.1.1. Temperature data

City-specific temperature datasets were obtained from regionalized observational sources covering a ten-year period (June–September). For Iași, daily mean and minimum air temperature rasters at 700 m resolution were provided by the University of Iași [85] for the period 2013–2022. For Jena, 30-min temperature fields at 25 m resolution were provided by the Thuringian State Office for the Environment, Mining and Nature Conservation (TLUBN) for 2021–2023. For Turku, air-temperature records from 57 fixed loggers spanning 2014–2023 were obtained from the University of Turku from the TURCLIM research group. Together, these datasets provide consistent, observation-based temperature fields suitable for the derivation of heat-hazard indicators at high spatial resolution.

3.1.2. Apartment rent

Geolocated apartment rent listings were collected from leading national online platforms, representing local housing markets in each city. The data include imobiliare.ro for Iași (1239 listings, August 2023), immowelt.de for Jena (1984 listings, April 2021 – January 2024), and vuokraovi.fi for Turku (9135 listings, January 2023 – June 2024). To enable cross-country comparison of socioeconomic indicators, information on national median equivalized net income was retrieved from Eurostat [86] (update 16 June 2025: Finland € 2391; Germany € 2302; Romania € 653). These datasets jointly form the basis for the construction of city-specific indicator of adaptive capacity and vulnerability.

3.1.3. Residential population

Population distribution data were derived from the Eurostat GEOSTAT 2021 population grid (1 km resolution). To represent the built environment, we used the DBSM R2023 conflated building-footprint dataset [87] and the Copernicus Building Height Model 2012 (v3, 10 m) [88]. Together, these layers provide harmonised, open-access information on buildings, forming a consistent basis for estimating residential population across the three study cities.

3.1.4. Land cover and green infrastructure

The land cover was characterized using Copernicus and Urban Atlas datasets. Specifically, we used the Tree Cover Density 2021 [89], Imperviousness 2018 [90] and Grassland [91] rasters at 100 m resolution from Copernicus. These data provide standardized, high-resolution information on vegetation cover and built-up structure within and across European cities.

3.1.5. Spatial extent and delineation

To ensure comparability and analytical consistency, the study area for each city was delineated using the Copernicus Urban Atlas 2018 [92]. We selected features and data within the Urban Core boundary and further restricted the analysis to built-up and residential land-use classes, including Discontinuous very low–to–dense urban fabric (< 10%–80% sealing level (S.L.)), Continuous urban fabric (> 80% S.L.), and Industrial, commercial, public, military and private units. This selection focuses the analysis on inhabited, structurally dense urban zones where heat exposure and vulnerability are most relevant. The delineation ensures that all datasets and subsequent analyses refer to comparable urban contexts across the three cities.

3.2. Methodology

3.2.1. Harmonization and analysis mask

All datasets were reprojected to the common equal-area projection EPSG:3035 and resampled to a 100 m grid. The spatial analysis was constrained to an urban residential mask derived from the Copernicus Urban Atlas 2018. We first selected all features belonging to the “Urban Core” and then restricted the extent further to land-use classes representing built-up residential and mixed-use areas, including: Discontinuous very low, low, medium, and dense urban fabric (S.L. <10%, 10–30%, 30–50%, 50–80%), Continuous urban fabric (S.L. >80%) and Industrial, commercial, public, military, and private units.

Only grid cells intersecting these classes and containing non-zero downscaled population were retained. This mask defines the inhabited, structurally dense urban fabric where heat exposure and risk are substantively relevant. All component layers, risk metrics, and figures were computed and reported within this spatial domain; blank areas in maps indicate regions outside the analysis extent.

3.2.2. Risk framework

We follow the IPCC risk framing [93] and first state the standard multiplicative form, which is widely applied in risk assessments [94–96].

$$R = H \times E \times V \tag{1}$$

where R is societal heat risk (unitless), H the thermal hazard, E exposure (residential population), and V vulnerability (susceptibility and lack of capacity).

We adopt an inverse vulnerability formulation, where risk increases with decreasing C (adaptive capacity) and compute day- and night-specific risk as:

$$R_{day} = H_{day} \times E \times (1 - C) \tag{2}$$

$$R_{night} = H_{night} \times E \times (1 - C) \tag{3}$$

In addition to societal risk, we compute per-capita, defined as:

$$R_{\text{cap}} = H \times (1 - C) \tag{4}$$

This component represents the per-capita risk potential arising from thermal hazard and vulnerability while holding exposure constant, and is not intended to capture psychological, behavioral, or perception-based individual risk.

In quantitative risk analysis, this distinction parallels the established separation between individual and societal risk, where individual risk describes the hazard-vulnerability relationship independent of population size [97]. Accordingly, we treat R_{cap} as a structural element of the risk framework that helps disentangle the relative contributions of hazard and adaptive capacity.

Before computing risk, all component rasters were harmonised to a common 100 m grid and scaled to a 0–1 range: hazard and exposure layers were divided by their city-specific maxima, and the rent-based adaptive-capacity layer was normalized using national median equivalised net income.

3.2.3. Hazard

Hazard (H) was quantified using two temperature-based indicators representing daily and nighttime thermal stress:

1. Temperature days (H_{day}) – days with daily mean temperature ≥ 20 °C
2. Tropical nights (H_{night}) – nights with minimum temperature ≥ 20 °C between 20:00 and 08:00 local time

Both indicators were expressed as mean annual counts for the period June–September over ten years (Iași 2013–2022; Jena 2014–2023; Turku 2014–2023), a suitable timeframe for such investigation [98].

Temperature data were processed city-specifically:

- Iași: Daily mean and minimimun air temperature rasters (700 m) for 2013–2022 were downscaled to 100 m using a linear dry-adiabatic lapse rate of 10 K km^{-1} and then filtered based on the thermal indicators of this study.
- Jena: Half-hourly 25 m rasters from TLUBN were aggregated to daily means and resampled to 100 m. As the provided data only covered 2021–2023, we hindcasted 2014–2020 using pixel-wise linear regressions ($R^2 > 0.8$) against local weather station data.
- Turku: Half-hourly air temperatures from 57 fixed loggers were aggregated to daily and nightly means and then regionalized using kriging with external drift (KED), with predictors including distance to the coast, local impervious fraction, and tree cover density within 100 m [72].

Given the evidence that elevated temperatures can trigger acute health impacts within just a few days, individual days were selected as the analytical unit instead of heatwave periods [99]. The 20 °C threshold for temperature days was chosen based on epidemiological findings from Finland and Romania that indicate increased mortality above this temperature [18,84,100,101]. According to the Finnish Meteorological Institute (FMI), hot days are characterized by a daily maximum temperature exceeding 27 °C and a daily mean temperature above 20 °C [102]. These thresholds are used in official heat warnings aimed at protecting vulnerable populations and outdoor workers. While the present study adopts the 20 °C daily mean threshold in line with prior epidemiological findings from Finland, the FMI's classification supports the relevance of this value for operational heat risk communication in Northern Europe. Although no equivalent threshold is defined for Germany, the Robert Koch Institute (RKI) considers extended periods with daily means ≥20 °C in its heat assessments [103], while other studies from Germany suggest thresholds for heat-related mortality between 19 °C and 22 °C [19,99,104].

3.2.4. Exposure

Exposure (E) was defined as the residential population distribution at 100 m resolution. Eurostat GEOSTAT 2021 population counts (1 km) were downscaled proportionally using a residential building-volume proxy [105] derived from building footprints and height data. For each cell c, total residential building volume was estimated as:

$$V_c = A_{\text{footprint},c} \times \bar{h} \tag{5}$$

where $A_{\text{footprint},c}$ is the total footprint area and $\bar{h}$ the mean height from Copernicus.

Population within each city was then allocated from the 1 km grid proportionally to V_c, yielding a continuous surface of residential exposure normalized to [0,1].

This approach provides a reproducible method for estimating high-resolution population distribution using openly available geospatial datasets [105]. We are focusing explicitly on inhabited built-up areas, ensuring that exposure reflects where people reside and sleep, consistent with the night-time hazard emphasis and the vulnerability concept used here [15,95,106].

3.2.5. Vulnerability and adaptive capacity

Adaptive capacity (C) was operationalized using geolocated apartment rents. Following best practices for data collection via web-scraping [107–110], listings were scraped from national real-estate platforms, and only entries with valid geolocation and complete pricing information were retained. Outliers and spatially unreliable records were removed.

Spatially continuous rent surfaces were generated via kriging with external drift (KED) [111,112], using exponential semivariogram models with city-specific nugget-to-sill ratios and practical ranges. Predictor variables included:

- Euclidean distances to the city center, public transport, supermarkets, and parks (OpenStreetMap, [113])
- Fraction of impervious surface, grassland and tree cover density within 100 m (Copernicus Landcover Monitoring Service, EEA, [89–91])
- Euclidean distance to the sea (Turku only)

These predictors were selected based on their demonstrated relevance for explaining spatial variation in housing markets and rental patterns [114–120].

To obtain adaptive capacity, monthly rents were normalized by the national median equivalised net income (Eurostat, 2025 update: Finland 2391€; Germany 2302€; Romania 653€), resulting in a dimensionless relative-rent measure.

The resulting adaptive-capacity layer C reflects relative socioeconomic and housing-related resilience, with higher values indicating greater capacity. Vulnerability was then defined directly from adaptive capacity as $V = 1 - C$ for use in the risk formulation.

This is justified because vulnerability is closely linked to adaptive capacity, in risk assessment, and understood as the economic, social, and material resources that enable people to manage and recover from environmental stress [121]. Vulnerability does not indicate the absence of capacity but rather a relative deficit of it, meaning that lower adaptive capacity manifests as higher vulnerability.

We use apartment rent in this context as it reflects key socioeconomic and housing-related factors that shape heat resilience. Rent levels are closely linked to household income [119], which determines access to protective resources and the capacity to cope with heat. Higher-rent areas are more likely to contain dwellings with better insulation, some degree of cooling infrastructure, and greater flexibility to use cooler interior spaces, whereas lower-rent housing is often associated with poorer thermal performance and limited options for reducing indoor heat [122–124].

Rent also captures affordability constraints: rental burden disproportionately affects low-income households [123,125,126], reducing their ability to invest in adaptive measures—such as fans or portable cooling—and increasing the likelihood of living in overcrowded or thermally inadequate dwellings [53,127]. Lower rents may further indicate older or less renovated building stock, where insufficient insulation and ventilation contribute to elevated indoor heat exposure, discomfort, and heat-related health risks during warm periods [29,34,35].

3.2.6. Land cover and green infrastructure

To characterise the environmental context of inhabited grid cells, we used Copernicus 100 m raster layers of tree cover density (2021), imperviousness (2018), and grassland (2018). The analysis was based on inhabited 100 m grid cells. For each inhabited cell, we calculated the relative share of each landcover class at two spatial scales: within the 100 m grid cell itself and within a 300 m circular buffer centred on the grid-cell centroid. The 100 m scale represents the immediate surroundings of each inhabited cell, whereas the 300 m buffer captures the broader neighbourhood context commonly used in urban studies [42,128]. These buffers are not intended to imply uniform cooling effects at these distances, but rather describe both local and near-neighbourhood environmental conditions around each dwelling.

Given that green infrastructure can influence thermal conditions [29,39,129] and is often unevenly distributed within cities [32–34,36], we examined statistical associations between land cover and the components of heat risk, without assuming causal relationships. Associations between risk components and landcover variables were quantified using Spearman rank correlations, chosen for their robustness to non-linearity and non-normality. To assess potential inequalities in both risk and green infrastructure, we computed Lorenz curves and Gini coefficients. Lorenz curves depict the cumulative share of a variable (e.g. risk) versus the cumulative share of urban residential areas in each city. A diagonal line indicates a uniform distribution, while deviations from this line reflect a degree of inequality. The Gini coefficient, ranging from 0 (perfect equality) to 1 (complete inequality), summarises this distribution numerically and has been widely applied in similar urban-environmental contexts [127].

4. Results

4.1. Exploratory statistics

Regarding hazard (Fig. 2), Iași exhibits the highest average number of temperature days and tropical nights, followed by Jena, while Turku shows the lowest overall heat exposure. The spatial distribution of temperature days is relatively similar across all three cities, although Iași displays slightly greater variability. In contrast, tropical nights are more unevenly distributed, particularly in Iași, where extensive urban areas are affected by elevated nighttime temperatures.

The residential population (Fig. 2) shows a comparable spatial pattern in all cities, characterized by a peak below 50 inhabitants per 10,000 m^2. Within this low-density range, Turku emerges as the least densely populated city, indicating lower potential exposure in large parts of its urban fabric.

For normalized apartment rent (Fig. 2), Iași shows the highest relative rent, with most values ranging between 0.3 and 0.6. In contrast, Jena and Turku mostly remain below 0.3. These patterns reflect substantial socioeconomic disparities between the cities, with direct implications for residents' vulnerability and adaptive capacity.

4.2. Land cover distribution

Fig. 3 shows the relative share of selected land-cover classes within the 100 m grid cells and the 300 m buffers surrounding inhabited locations. Tree cover is lowest in Iași, accounting for 7.6% (100 m cell) and 10.6% (300 m buffer) of the analysis area. Jena exhibits similarly low tree cover values. Turku, by contrast, has roughly double the amount of tree cover at both scales, with 20.5% and 22.2%, respectively.

Impervious surfaces dominate the local environment in Jena, reaching 47.2% within the 100 m cells and 36.8% within the 300 m buffers. Turku ranks second in imperviousness and Iași third, with both cities showing approximately two-thirds of Jena's values at the local scale.

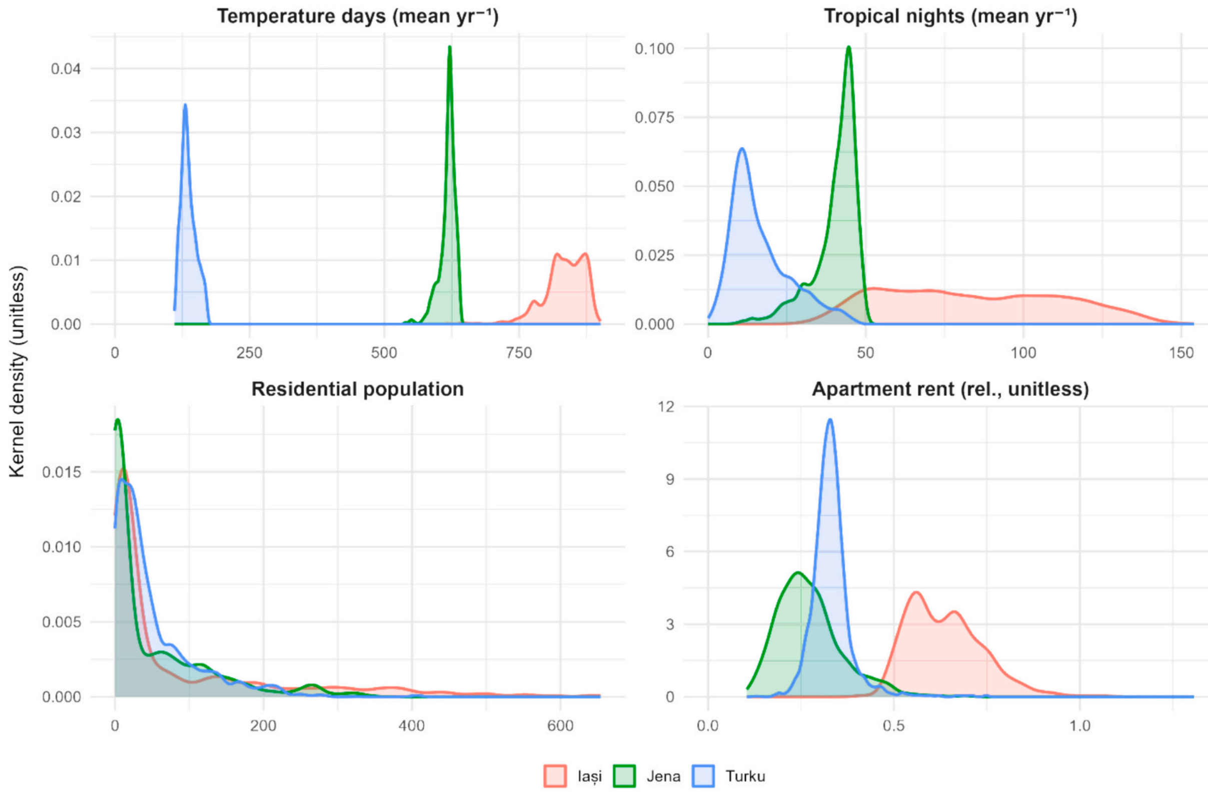

Fig. 2. Kernel density distributions of risk components by city. Temperature days (mean yr^{-1}), Tropical nights (mean yr^{-1}), Residential population, Apartment rent (rel., unitless).

Fig. 3. Mean relative share of selected land cover classes (tree cover, impervious surface, and grassland) across all inhabited areas in Iași, Jena, and Turku. To capture different spatial contexts, the analysis compares two scales: the immediate local environment within the respective 100 m inhabited grid cells (left) and the broader neighbourhood context captured by a 300 m circular buffer around the grid-cell centroids (right). Values do not sum to 100% as other land-cover classes (e.g., water bodies, bare soil) are excluded from this visualization.

Grassland shares are remarkably similar across all three cities. Within the 100 m cells, grassland accounts for approximately 10–11% of the analysis area in each city, and within the 300 m buffers, it increases slightly to about 13–14%. This indicates that, unlike tree cover or impervious surfaces, grassland availability around inhabited areas is relatively consistent across the three differing urban contexts.

Fig. 4 shows Lorenz curves and Gini coefficients that summarise the spatial distribution of green and built surfaces across the three cities. All land-cover types exhibit spatial inequality, but the magnitude and direction differ across cities and scales. Tree cover is most evenly distributed in Turku (Gini = 0.44 at 100 m; 0.47 at 300 m), whereas Iași displays the strongest inequality (0.76 at both scales). Jena shows

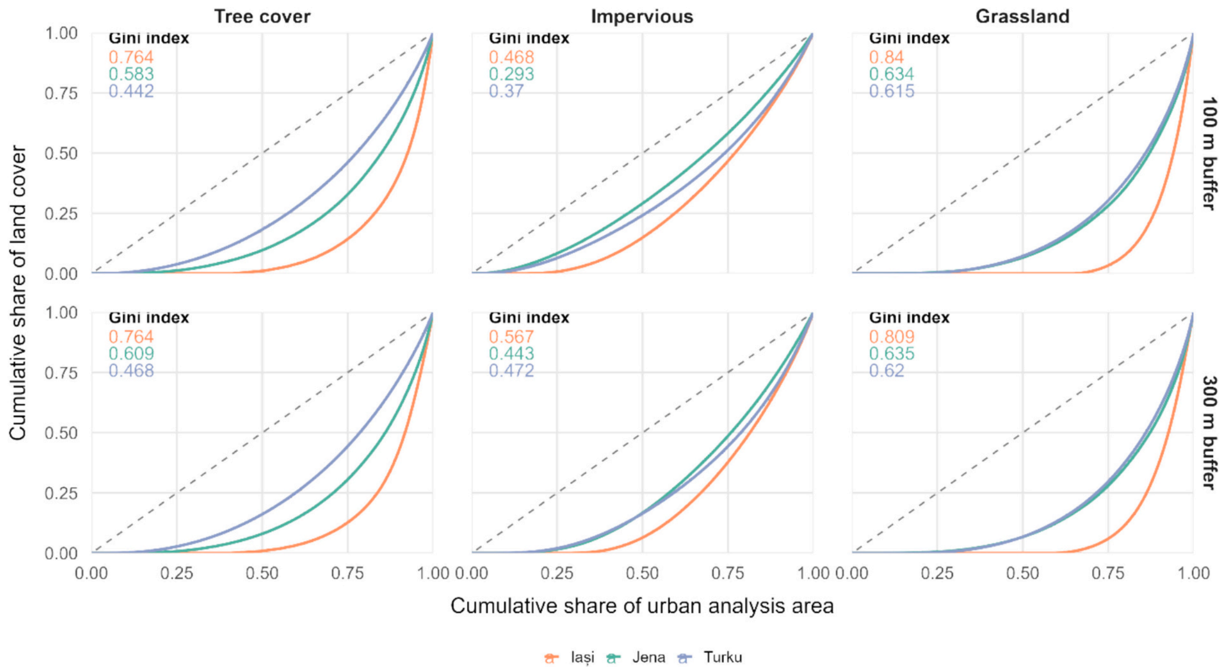

Fig. 4. Lorenz curves and Gini coefficients illustrating the equality in spatial distribution of land cover variables – grassland, tree cover density, and impervious surfaces - at both the local (100 m) and neighbourhood (300 m) scale for Iași, Jena, and Turku.

intermediate values (0.58 at 100 m; 0.61 at 300 m), with only minor scale-related changes.

Grassland also exhibits substantial inequality in all three cities. Iași shows the highest Gini values (0.84 at 100 m; 0.81 at 300 m), indicating that grassland is concentrated in a small portion of the analysis area. Jena and Turku show lower but still pronounced inequalities (≈0.63–0.64 across both scales), with little change between the local (100 m) and neighbourhood (300 m) contexts. These results reflect the strongly clustered distribution of grassland within urbanised areas.

Impervious surfaces show patterns nearly opposite to those of vegetation. Jena exhibits the most even distribution of imperviousness (0.29 at 100 m; 0.44 at 300 m), while Iași and Turku show stronger inequalities, particularly at the local scale (Iași 0.47; Turku 0.37). At 300 m, inequality increases in both Iași (0.57) and Turku (0.47), indicating that built-up areas become more spatially concentrated when viewed at neighbourhood scale.

Overall, these results demonstrate that vegetation – both tree cover and grassland - is substantially more unevenly distributed than impervious surfaces in all cities. Iași consistently exhibits the strongest spatial concentration of both vegetation types, whereas Turku shows the most balanced tree-cover distribution and Jena the most homogeneous imperviousness pattern. Differences between the 100 m and 300 m scales are modest, indicating that spatial inequalities in urban land cover persist across local and neighbourhood contexts.

A complete set of correlations between hazard, exposure, vulnerability and land cover is provided in Supplementary Fig. S1. Daytime and nighttime hazard metrics are positively correlated in all cities, although the strength of this relationship differs. In Iași, Temperature Days and Tropical Nights show strong coupling ($\rho \approx 0.83$), indicating that hot days and warm nights frequently co-occur. Both hazard metrics exhibit moderate negative correlations with apartment rent ($\rho \approx -0.47$ and -0.37), suggesting that higher-rent areas tend to experience slightly lower temperatures. Hazard–land-cover relationships are weak at 100 m but more pronounced at 300 m: tree cover and grassland correlate negatively with daytime hazard (down to −0.30), while imperviousness shows moderate positive correlations (up to 0.50). Nighttime hazard follows similar but generally weaker patterns. Vegetation types correlate negatively with imperviousness ($\rho \approx -0.50$ to −0.71), and tree cover and grassland are moderately positively correlated at 300 m ($\rho \approx 0.50$). Population–hazard associations are weak to moderate.

In Jena, Temperature Days and Tropical Nights are moderately correlated ($\rho \approx 0.54$), reflecting weaker day–night coupling than in Iași. Associations between hazard and apartment rent are small and positive ($\rho \approx 0.13$–0.16), indicating limited alignment between thermal conditions and socioeconomic patterns. Hazard–land-cover relationships show the expected physical signal: vegetation correlates negatively with both daytime and nighttime hazard (−0.30 to −0.45), while imperviousness correlates positively (≈ 0.60). Tree cover shows a stronger negative relationship with daytime heat, whereas grassland correlates more strongly with nighttime heat. Vegetation and imperviousness are strongly inversely correlated at 100 m (≈ −0.70). Population shows low to moderate associations with hazard, increasing for nighttime conditions.

Turku exhibits the strongest day–night hazard similarity of the three cities ($\rho \approx 0.77$). Hazard–rent associations are small and negative (≈ −0.22 to −0.26), indicating that slightly cooler areas tend to coincide with higher rents. Hazard–land-cover relationships resemble those in Iași and Jena but are more pronounced: tree cover correlates moderately with lower daytime heat (≈ −0.50) and strongly with lower nighttime heat (≈ −0.60 to −0.74). Imperviousness shows moderate to strong positive associations with hazard, particularly at night. As in the other cities, vegetation and imperviousness are negatively correlated, with moderate to strong inverse relationships at both scales.

4.3. Urban heat-related risk patterns

Fig. 5 shows the spatial distribution of societal heat risk across the three study cities. In Iași, the highest societal risk occurs in the central and western districts, which comprise dense mixed-use neighbourhoods, the university area, and extensive residential blocks. In Jena, elevated societal risk is concentrated in the large housing estates of Lobeda (south) and Winzerla (west), both characterized by high residential densities and predominantly lower- to middle-income populations. In Turku, the highest values cluster in the inner city, where compact mixed-use structures and substantial economic activity coincide with limited vegetation. Across all cities, these high-risk zones generally

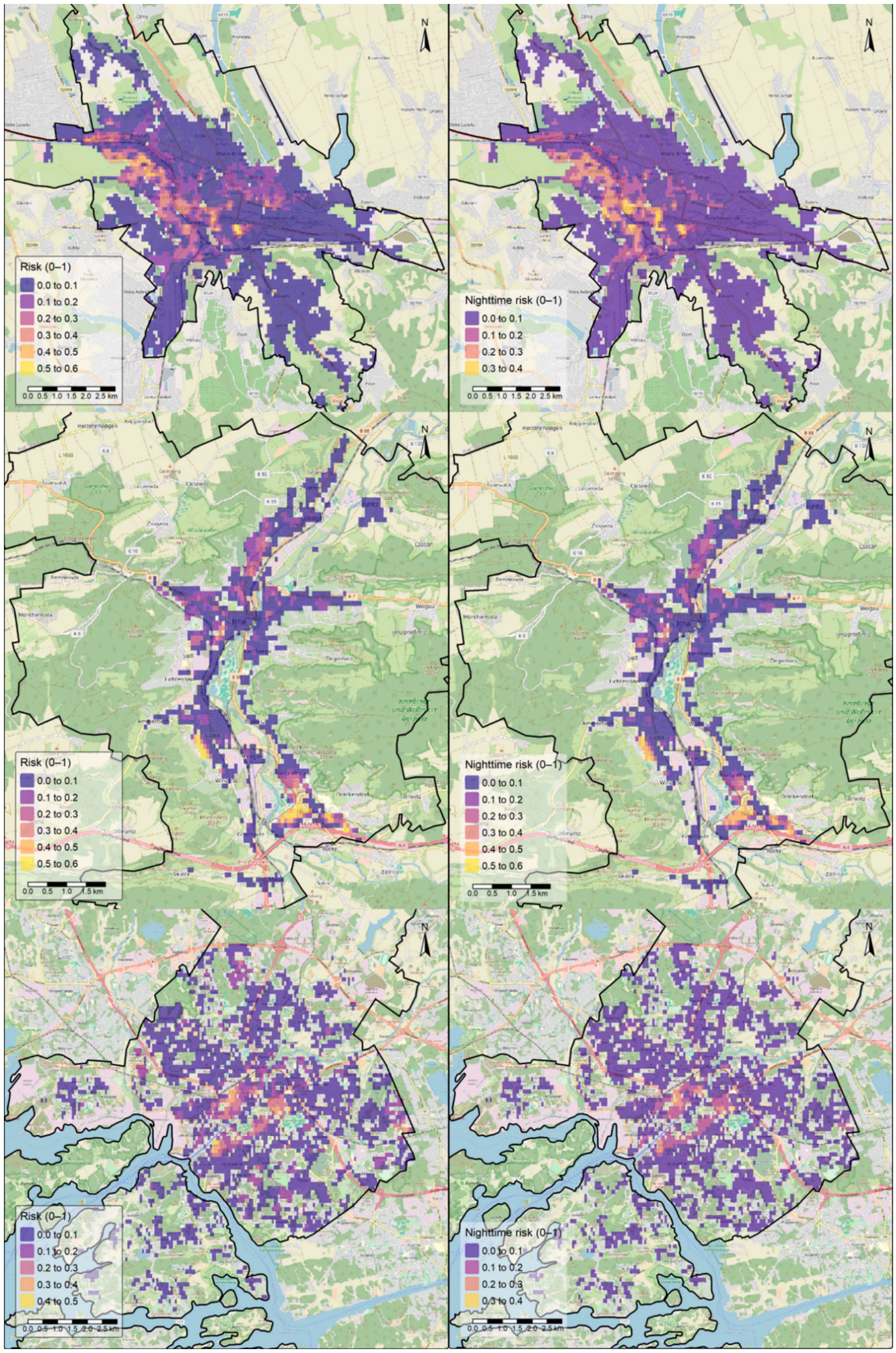

Fig. 5. Societal heat-risk maps at 100 m resolution for the three cities - top: Iași, middle: Jena, bottom: Turku. The left column shows daytime societal risk; the right column shows nighttime societal risk. Urban core boundaries are shown as black outlines. Maps are masked to populated residential and mixed-use areas; blank areas indicate non-residential or no-value cells. Absolute values are not directly comparable across cities because risk components were max-scaled within each city.

correspond to strongly built-up areas with comparatively low vegetation cover.

Within all cities, societal heat risk is shaped predominantly by the distribution of residential population, resulting in distinct and stable hot spots (Fig. 6). This dominance of exposure is reflected in the near-perfect correlations between population and both daytime and nighttime societal risk ($\rho \approx 0.93$–0.99). Thus, areas with high societal risk are primarily those where many inhabitants are concentrated, largely independent of local thermal variability. As a consequence, daytime and nighttime societal-risk maps are highly similar; in Iași, for example, they are almost identical ($\rho \approx 0.99$), with similarly high diurnal consistency in Jena and Turku.

Thermal hazard contributes to spatial variation in societal risk, though to a more modest extent. In Iași, societal risk correlates moderately with both Temperature Days and Tropical Nights ($\rho \approx 0.30$–0.50), while in Jena and Turku these relationships are weaker and typically below 0.40. Associations with vulnerability are consistently negative but small (≈ -0.20), indicating that higher-rent areas tend to show slightly lower societal risk; however, this influence is minor compared with the overwhelming effect of population distribution. Societal heat risk should therefore be interpreted primarily as a measure of where many people live relative to hazardous thermal conditions, rather than a direct

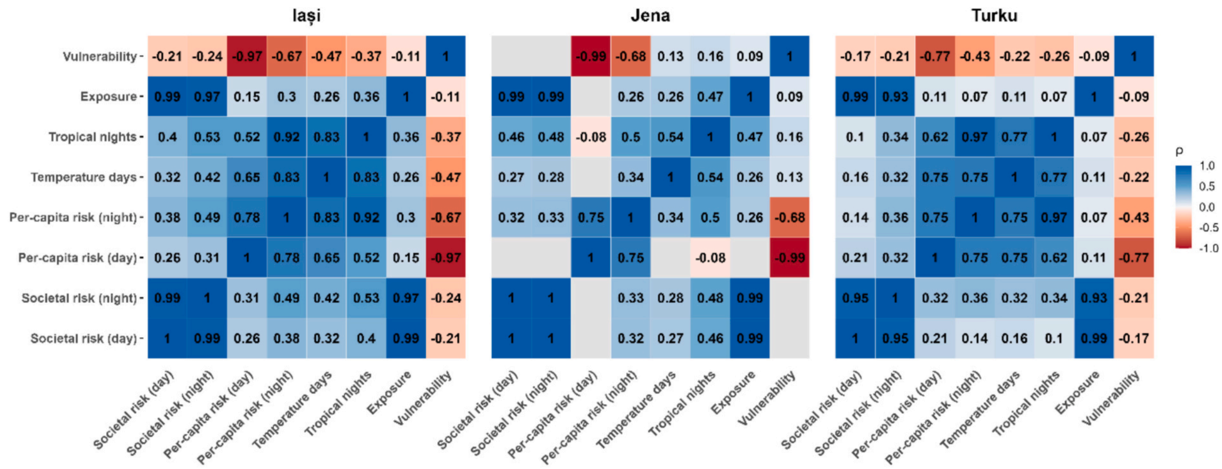

Fig. 6. Spearman correlation matrices of the risk components – hazard, exposure, vulnerability, and the resulting risk metrics (societal risk: daytime and nighttime; per-capita risk: daytime and nighttime) - for Iași, Jena, and Turku. Each matrix shows pairwise correlation coefficients (ρ), where red indicates negative and blue positive relationships. In all cities, residential population is almost perfectly correlated with societal risk (ρ ≈ 0.99), whereas the relationships between hazard, vulnerability, and per-capita risk vary by context. Only correlations that are significant at a nominal α level of 0.05 are shown (*t*-tests, no adjustment for multiplicity).

reflection of socio-economic sensitivity.

To complement this aggregated perspective, per-capita risk isolates the contribution of hazard and vulnerability by holding exposure constant (Fig. S2). In Iași, per-capita risk correlates moderately with daytime hazard but becomes strongly aligned with nighttime conditions (ρ ≈ 0.83 for Temperature Days; ρ ≈ 0.92 for Tropical Nights). Exposure, by definition, contributes little (ρ ≈ 0.15–0.30). Most notable is the very strong negative association with vulnerability: per-capita risk correlates with rent at −0.97 (day) and − 0.67 (night), indicating that residents in lower-rent areas face substantially higher individual heat burden.

Jena shows a similar but more pronounced pattern. Daytime per-capita risk has no meaningful association with Temperature Days or exposure but exhibits an almost perfect negative correlation with vulnerability (ρ ≈ −0.99). Nighttime per-capita risk becomes more responsive to hazard (ρ ≈ 0.34–0.50), while correlations with exposure remain weak (ρ ≈ 0.26). The negative association with rent (ρ ≈ −0.68)

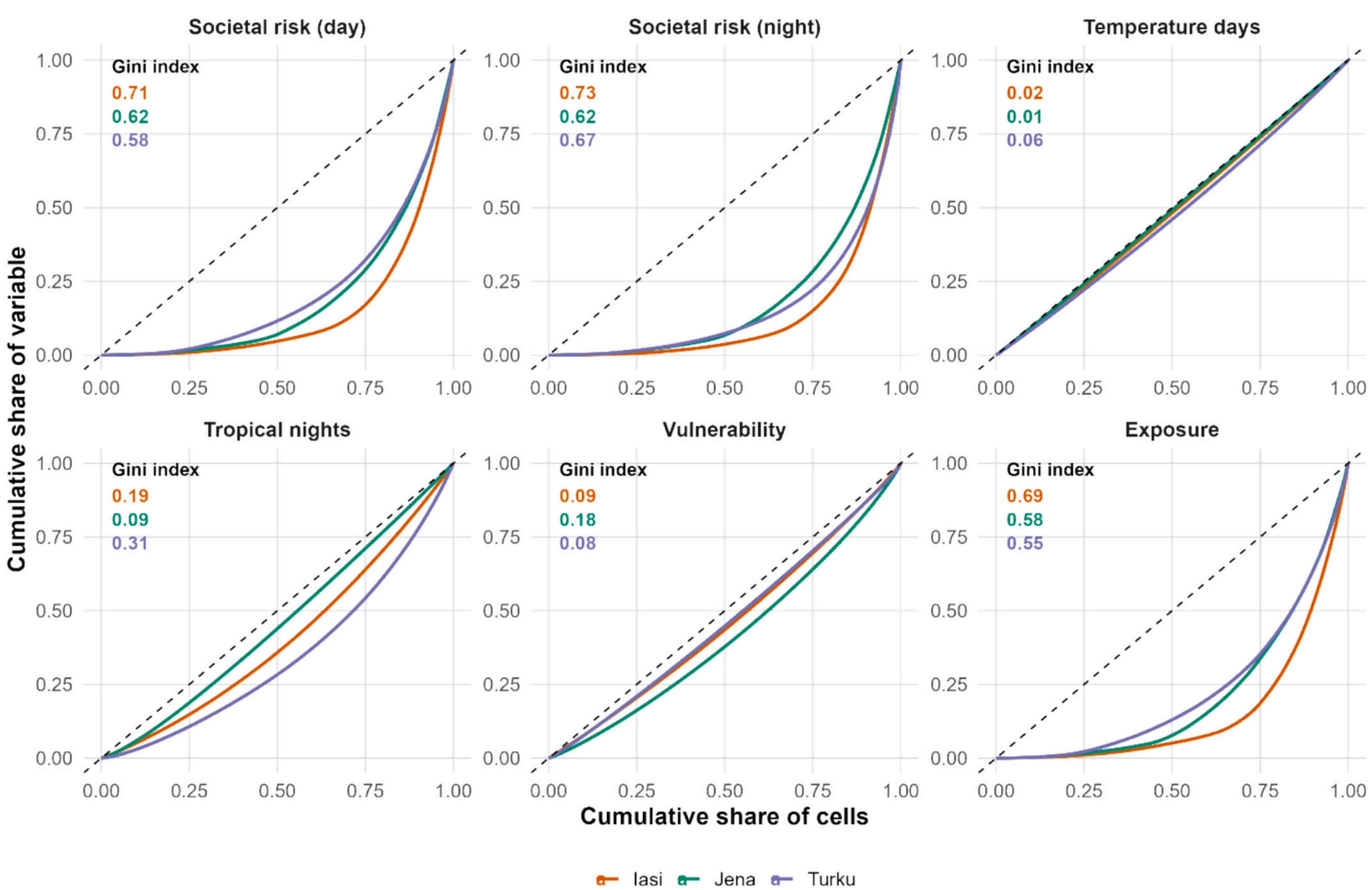

Fig. 7. Lorenz curves illustrating the spatial distribution of daytime and nighttime risk, as well as the individual unscaled components. Gini indices are shown within each plot and quantify the degree of inequality. The curves highlight unequal distribution patterns, particularly for Tropical Nights and Exposure.

demonstrates that socio-economic disparities strongly shape individual heat burden in Jena, even though their imprint on societal risk remains modest.

In Turku, per-capita risk is consistently driven by thermal hazard. Daytime values correlate moderately to strongly with Temperature Days and Tropical Nights (ρ ≈ 0.62–0.75), and nighttime per-capita risk exhibits very strong correlations with nighttime hazard (up to ρ ≈ 0.97). Exposure contributes minimally (ρ ≈ 0.07–0.11). Negative correlations with vulnerability remain substantial (ρ ≈ −0.43 to −0.77), though generally weaker than in Iași and Jena.

Additional correlations between risk components and land cover are provided in Supplementary Fig. S3.

4.4. Spatial inequalities of risk and its components

Lorenz curves and Gini indices (Fig. 7) illustrate the degree of spatial inequality in societal heat risk and its components, revealing substantial differences among the three cities. Daytime societal risk is strongly concentrated in all cases, with Iași showing the highest inequality (Gini = 0.71) and Jena (0.62) and Turku (0.58) somewhat lower but still pronounced disparities. Nighttime societal risk follows a similar pattern; however, inequality increases markedly in Turku (Gini = 0.67), indicating a more uneven distribution of nocturnal risk. These patterns are consistent with the risk maps, where a small number of densely populated hot spots exhibit very high risk values, while large parts of the urban area show comparatively uniform and low risk.

This pronounced inequality in societal risk mirrors the distribution of exposure—identified in the previous section as the dominant component of societal risk. High Gini values for both risk and exposure underscore their close relationship.

In contrast, daytime hazard is distributed almost uniformly within each city. Lorenz curves lie close to the line of equality, resulting in low Gini coefficients and indicating that neither the hilly topographies of Iași and Jena nor the coastal setting of Turku generate substantial spatial disparities in daytime thermal hazard.

Nighttime hazard presents a different picture, with significantly greater inequality, particularly in Iași and Turku. Here, elevated nocturnal temperatures are concentrated in specific urban areas, reflecting stronger spatial structuring of nighttime thermal environments.

Vulnerability, operationalized via apartment rent, is comparatively evenly distributed across all cities. Jena is an exception, showing a more unequal pattern likely related to contrasts between high-rent hillside districts near the city centre and lower-rent areas such as Lobeda.

Overall, these findings demonstrate that spatial inequalities in societal heat risk are primarily shaped by exposure, with additional contributions from nighttime hazard—especially in Iași and Turku—and, to a lesser extent, from socio-economic vulnerability, most notably in Jena.

Results for per-capita risk and its components are provided in Supplementary Fig. S4.

5. Discussion

Within all three cities, the spatial patterns of societal risk are shaped predominantly by the distribution of residential population. Our analysis shows a clear divergence between societal and per-capita heat risk. Societal risk closely mirrors the spatial distribution of residents, with only modest modulation by thermal hazard and a weak imprint of socioeconomic vulnerability. In contrast, per-capita risk, aligns much more strongly with hazard intensity and, most notably, with socioeconomic vulnerability, revealing patterns that remain largely masked in the population-weighted societal metric.

Heat-risk studies support this finding globally [130] and at city scale [131]. Prior work shows that aggregated societal risk patterns at the city scale largely follow the spatial distribution of population, while differences in hazard intensity – whether daytime maxima or nighttime minima - modulate rather than determine the overall pattern [54,132,133] (e.g., Seoul, Phoenix, Philadelphia). Even when daytime and nighttime thermal fields differ, the broad structure of societal risk often remains similar because risk “moves with people”: high daytime exposure in employment centres and high nighttime exposure in dense residential neighbourhoods [20].

These studies further demonstrate that socioeconomic vulnerability tends to alter the magnitude of risk within exposed areas but rarely reshapes the citywide spatial footprint of societal risk once population distribution is accounted for [54]. This aligns with our results: hazard contributes modestly, and vulnerability only weakly, while exposure overwhelmingly dominates the spatial pattern of societal risk in all three cities. Looking at individual-level and per-capita heat-risk studies, we see that the geography of heat risk becomes more tightly linked to hazard intensity and socioeconomic conditions [134,135]. Evidence from epidemiological and urban climate research indicates that low-income or low-rent areas systematically experience higher individual heat burden – even under the same citywide heat event - because housing quality, microclimatic conditions, and limited cooling options accentuate exposure at the person level [55,136]. This is particularly pronounced for nighttime conditions, where elevated minimum temperatures and poor indoor thermal performance compound individual heat stress [137,138]. The strong negative correlations between per-capita risk and rent in Iași, Jena, and Turku may reflect these broader patterns.

A key finding in our study is that nighttime hazard exerts a stronger influence on both societal and per-capita risk than daytime heat. This is particularly evident in Turku and Iași, where Tropical Nights show greater spatial heterogeneity and stronger association. The temperature generation and distribution within the cities is well studied. In Iași, the patterns are consistent with previous urban-climate studies that document a pronounced summer urban heat island, with nocturnal air-temperature differences of around 2.5–4 °C between inner-city and rural sites and persistent warm anomalies during heat-prone periods [139,140]. Mobile transect measurements further show that topography plays a decisive role: strong cold-air drainage along valley floors and thermal inversions below ~400 m altitude create local cooling pockets of 3–5 °C, fragmenting the UHI into multiple warm cores [66].

In Jena, the dominance of exposure in shaping societal risk and the strong role of vulnerability in per-capita risk reflect its characteristic valley morphology and documented thermal behavior. Climate-planning studies identify Jena as one of the warmest cities in central Germany, partly because the Saale valley and surrounding limestone slopes store heat and limit nocturnal ventilation [69]. Projections indicate strong increases in hot days and nighttime heat stress (tropical nights) by the end of the century [71], and municipal assessments emphasise that heat-risk patterns are most pronounced in large housing estates such as Lobeda and Winzerla.

In Turku studies show that maritime influences and sea-breeze penetration frequently produce daytime urban cool-island effects in spring and summer, whereas a robust nighttime UHI persists year-round, averaging ~2 °C and occasionally reaching 4–10 °C in summer [73].

These findings are of high importance with extensive public health research showing that nighttime minimum temperatures have independent, and often stronger, effects on heat-related morbidity and mortality, even after adjusting for daytime heat [137,141,142]. Mechanistically, this is well understood. Physiological recovery primarily occurs at night, and several controlled-environment studies demonstrate that elevated nighttime temperatures reduce sleep duration, prevent thermoregulatory recovery, and maintain elevated core body temperature into the daytime, thereby compounding cardiovascular strain [143]. Crucially, individuals experience nighttime heat indoors, where temperatures often track or exceed outdoor minima [144]. Studies show that indoor temperature dynamics depend strongly on insulation, shading, ventilation, building orientation, and floor level [16,28]. Reviews of indoor overheating in Europe highlight that such conditions disproportionately impact older adults, low-income groups, and residents of social or rental housing without mechanical cooling [16]. Evidence from Jena underscores the behavioral dimension: vulnerable individuals tend to remain indoors on hot days and avoid public spaces [145].

Our results show that apartment rent functions as a proxy for environmental conditions that shape heat exposure. In Turku and Iași, higher rents are associated with more favourable microclimates – characterized by higher tree-cover density and lower imperviousness - which correspond to lower hazard levels and reduced heat risk. These patterns are consistent with extensive research from Europe and North America showing that higher-income or higher-price neighbourhoods tend to have more green infrastructure, less impervious surface, and lower ambient and indoor heat exposure, while lower-income or low-rent areas are systematically hotter and less green - a disparity often reflected in housing markets, where greener, cooler neighbourhoods command higher rents [37,119,129,146,147]. Within this broader context, the city-specific patterns observed in our results align well with international evidence.

Land cover patterns further modulate the geography of temperature patterns and consequently risk. Consistent with the urban climate literature, we observe negative correlations between green land cover (tree cover, grassland) and both hazard components, particularly during daytime when shading, evapotranspiration, and albedo effects are strongest [148]. Impervious surfaces, by contrast, show robust positive correlations with hazard and risk in all cities, in agreement with global evidence that built-up surfaces absorb and re-emit heat, elevating both daytime and nighttime temperatures [149]. Finally, our inequality analysis shows that green space availability is unevenly distributed, reflecting broader environmental-justice patterns [147,150–152]. In Jena, previous work has shown that although cooling green spaces are generally abundant, accessibility varies substantially, with vulnerable populations in northern districts facing reduced access to suitable green areas [145]. In Turku and Iași, green space is positively associated with apartment rent, while in Jena this pattern is less pronounced. Combined with the negative correlations between per-capita risk and vulnerability, these findings indicate that socio-economic disparities in heat risk are intertwined with disparities in availability of green infrastructure, though the strength and direction of these relationships differ across cities.

In addition to these empirical insights, the study offers several methodological contributions. It provides a comparative, high-resolution analysis across three European cities in different climatic and socioeconomic contexts, using a 100 m grid that captures intra-urban risk patterns more precisely than typical administrative units. The use of apartment rent as a vulnerability proxy introduces a flexible, fine-scale alternative to census-based data, which are often outdated or aggregated due to privacy constraints. The parallel assessment of societal and per-capita risk enables a nuanced distinction between aggregate population-level impacts and individual-level vulnerability. Finally, the use of ten years of observation-based, downscaled air-temperature data allows for a more realistic representation of both daytime and nighttime heat stress than approaches relying solely on satellite-derived land surface temperature.

6. Limitations and methodological considerations

While this study provides a high-resolution, multi-component analysis of urban heat risk across three European cities, several limitations should be acknowledged.

First, the regionalization of air temperature data was carried out using different methods across cities—ranging from kriging with external drift (KED) to random forest models and dry-adiabatic lapse rates. While each approach was selected based on data availability and local expertise, these methodological differences may affect intercity comparability. Future studies should aim to harmonize thermal modeling procedures or apply cross-city validation schemes.

Second, our analysis is based on outdoor air temperature as a proxy for heat exposure. While this may represent a meaningful approximation for outdoor and indoor conditions [82,144], we did not have information about indoor conditions, which may differ substantially depending on building quality, insulation, orientation, inhabitant behavior or vicinity to cooling infrastructure [26,144,153,154]. This limitation is particularly relevant at night, when people are indoors and nighttime heat stress becomes critical. The lack of spatially comprehensive indoor temperature data remains a general challenge in urban climate research and should be addressed in future studies using in-situ monitoring, smart home data, or building energy models.

Third, the study applies a uniform threshold of 20 °C to define both temperature days and tropical nights across all cities. While this facilitates cross-city comparison, it may underrepresent local physiological acclimatization and regional climatic baselines [11,18,155,156]. For example, the health implication of a 20 °C-day may differ between Turku and Iași. Future research could test the sensitivity of findings to alternative definitions.

Fourth, the use of apartment rent as a proxy for vulnerability remains context dependent. Moreover, scraped rental data reflect only the formal housing market and may underrepresent lower-income groups living in informal, subsidized, or non-standard housing arrangements. To address this, future research could include several sources of rental offer data and triangulate rent data with additional indicators such as energy poverty, building age, or census-based deprivation metrics.

Despite these limitations, the methodological framework presented here remains robust and adaptable. Future applications could benefit from integrating behavioral data [157], longitudinal analyses, and community-based validation [158–160]. Especially the use of rental data – as a widely accessible, spatially detailed, and flexible proxy - holds considerable potential for urban climate risk research, particularly in data-scarce or privacy-sensitive environments.

7. Conclusion

To our knowledge, this is the first study for each of the three cities to provide an integrated heat-risk assessment at this spatial resolution and conceptual detail – combining diurnally resolved hazard, exposure, and rent-based vulnerability - even though their urban heat islands have previously been described in detail. This study shows that urban heat risk in Iași, Jena, and Turku is shaped by distinct but interacting drivers. Societal risk is dominated by exposure: areas with high residential population consistently exhibit the highest aggregated risk, while spatial differences in temperature or vulnerability only modestly modify this pattern. In contrast, per-capita risk reveals inequalities that remain largely invisible at the societal scale, highlighting places where individuals face disproportionately high heat burden despite lower population density.

Across all cities, nighttime heat emerges as a particularly influential hazard component. Tropical Nights show stronger and more spatially variable associations with both societal and per-capita risk than daytime conditions, underscoring the importance of nocturnal cooling for recovery and health. Patterns of vulnerability also vary by context. Apartment rent – used here as a fine-scale proxy for socioeconomic conditions - aligns closely with per-capita risk in Iași and Turku, whereas in Jena this relationship is weaker and shaped by local topography and urban form. This highlights that vulnerability indicators derived from housing markets can be informative but must be interpreted within city-specific contexts.

Land cover further modulates spatial patterns of hazard and risk. Tree cover and grassland are consistently associated with lower daytime temperatures, while impervious surfaces intensify both daytime and nighttime conditions. The uneven distribution of green infrastructure mirrors broader socio-environmental inequalities and suggests that equitable access to cooling landscapes is still lacking, but essential for effective heat-adaptation planning.

By integrating high-resolution, observation-based temperature metrics with harmonised exposure and vulnerability indicators, this study provides a transferable framework for assessing urban heat risk in settings where detailed socioeconomic data are limited. The findings underscore the need for policies that jointly address population-level exposure, individual vulnerability, and the spatial distribution of environmental cooling resources.

Future work could build on this framework by incorporating indoor temperature measurements, alternative or complementary vulnerability indicators, especially building characteristics and heat-protective amenities, and longitudinal analyses to examine how risk patterns evolve under changing climatic and socioeconomic conditions.

CRediT authorship contribution statement

Pascal Schlechtweg: Writing – review & editing, Writing – original draft, Visualization, Software, Methodology, Formal analysis, Data curation, Conceptualization. **Alexander Brenning:** Writing – review & editing, Supervision, Resources, Methodology, Funding acquisition, Conceptualization. **Jukka Käyhkö:** Writing – review & editing, Supervision, Resources, Methodology, Funding acquisition, Conceptualization. **Lucian Sfîcă:** Writing – review & editing, Supervision, Resources, Methodology, Conceptualization.

Funding sources

Lucian Sfîcă was supported by a grant of the Ministry of Research, Innovation and Digitization, CNCS - UEFISCDI, project number PN-IV-P1-PCE-2023-0897, within PNCDI IV (Romania).

Declaration of competing interest

The authors declare that they have no known competing financial interests or personal relationships that could have appeared to influence the work reported in this paper.

Acknowledgements

The authors wish to thank all colleagues and institutions who contributed to this research, as well as the Thuringian State Office for Environment, Mining and Nature Conservation (TLUBN) for providing the temperature data for Jena. We also gratefully acknowledge EC2U for the network structure (Virtual Institute for Sustainable Cities and Communities (VISCC), EC2U – European Campus of Universities) and mobility opportunities that facilitated collaboration between the participating universities, including the Erasmus+ supported seed mobilities.

Appendix A. Supplementary data

Supplementary data to this article can be found online at https://doi.org/10.1016/j.cacint.2026.100415.

Data availability

The explanation is given in the manuscript.

References

[1] IPCC. Lee H., Romero J. editors. Sections. In: Climate Change 2023: Synthesis Report. Contribution of Working Groups I, II and III to the Sixth Assessment Report of the Intergovernmental Panel on Climate Change [Core Writing Team. Geneva, Switzerland: IPCC; 2023. p. 35–115. doi:10.59327/IPCC/AR6-9789291691647.
[2] World Meteorological Organization. WMO confirms 2024 as warmest year on record at about 1.55 °C above pre-industrial level. 2025.
[3] Copernicus. European State of the Climate 2022. 2023.
[4] Ballester J, et al. Heat-related mortality in Europe during the summer of 2022. Nat Med 2023;29(7):1857–66.
[5] European Environment Agency. Cooling buildings sustainably in Europe: exploring the links between climate change mitigation and adaptation, and their social impacts. 2022.
[6] Ward K, et al. Heat waves and urban heat islands in Europe: a review of relevant drivers. Sci Total Environ 2016;569:527–39.
[7] Rizwan AM, Dennis LY. A review on the generation, determination and mitigation of Urban Heat Island. J Environ Sci 2008;20(1):120–8.
[8] Ignjačević P, et al. Climate-induced mortality projections in Europe: estimation and valuation of heat-related deaths. International Journal of Disaster Risk Reduction 2024;111:104692.
[9] Elmarakby E, Elkadi H. Prioritising urban heat island mitigation interventions: mapping a heat risk index. Sci Total Environ 2024;948:174927.
[10] Ebi KL, et al. Hot weather and heat extremes: health risks. Lancet 2021;398 (10301):698–708.
[11] Kovats RS, Hajat S. Heat Stress and Public Health: A Critical Review. In: Annual Review of Public Health. **29**; 2008. p. 41–55.
[12] Santamouris M. Heat island research in Europe: the state of the art. Adv Build Energy Res 2007;1(1):123–50.
[13] Possega M, et al. Observational evidence of intensified nocturnal urban heat island during heatwaves in European cities. Environ Res Lett 2022;17(12): 124013.
[14] He C, et al. Nocturnal heat exposure and stroke risk. Eur Heart J 2024;45(24): 2158–66.
[15] Beckmann SK, Hiete M, Beck C. Threshold temperatures for subjective heat stress in urban apartments—analysing nocturnal bedroom temperatures during a heat wave in Germany. Clim Risk Manag 2021;32:100286.
[16] Kenny GP, et al. Indoor overheating: a review of vulnerabilities, causes, and strategies to prevent adverse human health outcomes during extreme heat events. Temperature 2024;11(3):203–46.
[17] Gallo E, et al. *Heat-related mortality in Europe during* 2023 and the role of adaptation in protecting health. Nat Med 2024:1–5.
[18] Kivimäki M, et al. Climate change, summer temperature, and heat-related mortality in finland: multicohort study with projections for a sustainable vs. fossil-fueled future to 2050. Environ Health Perspect 2023;131(12):127020.
[19] Winklmayr C, et al. Heat-Related Mortality in Germany From 1992 to 2021. Dtsch Arztebl Int 2022;119(26):451–7.
[20] Yoo C, et al. Diurnal urban heat risk assessment using extreme air temperatures and real-time population data in Seoul. Iscience 2023;26(11).
[21] Kim Y, Yoo C, Im J. Nighttime satellite land surface temperature for urban applications: achievements, challenges, and future prospects. GIScience & Remote Sensing 2025;62(1):2527990.
[22] Liu J, et al. Nonlinear exposure-response associations of daytime, nighttime, and day-night compound heatwaves with mortality amid climate change. Nat Commun 2025;16(1):635.
[23] Cheval S, et al. A systematic review of urban heat island and heat waves research (1991–2022). Clim Risk Manag 2024;44:100603.
[24] Brasche S, Bischof W. Daily time spent indoors in German homes – Baseline data for the assessment of indoor exposure of German occupants. Int J Hyg Environ Health 2005;208(4):247–53.
[25] Schweizer C, et al. Indoor time–microenvironment–activity patterns in seven regions of Europe. Journal of exposure science & environmental epidemiology 2007;17(2):170–81.
[26] Franck U, et al. Heat stress in urban areas. Indoor and outdoor temperatures in different urban structure types and subjectively reported well-being during a heat wave in the city of Leipzig. Meteorologische Zeitschrift (Berlin) 2013:22.
[27] Thomson H, et al. Energy poverty and indoor cooling: an overlooked issue in Europe. Energ Buildings 2019;196:21–9.
[28] Zuurbier M, et al. Street temperature and building characteristics as determinants of indoor heat exposure. Sci Total Environ 2021;766:144376.
[29] Taylor J, et al. Ten questions concerning residential overheating in central and northern Europe. Build Environ 2023;234:110154.
[30] Farahani AV, et al. Overheating assessment for apartments during average and hot summers in the Nordic climate. Build Res Inf 2024;52(3):273–91.
[31] Bonnefoy XR, et al. Housing and health in Europe: preliminary results of a pan-European study. Am J Public Health 2003;93(9):1559–63.
[32] Braubach M, Fairburn J. Social inequities in environmental risks associated with housing and residential location—a review of evidence. European journal of public health 2010;20(1):36–42.
[33] Seebass K. Who is feeling the heat?: vulnerabilities and exposures to heat stress—individual, social, and housing explanations. Nat Culture 2017;12(2): 137–61.
[34] Samuelson H, et al. Housing as a critical determinant of heat vulnerability and health. Sci Total Environ 2020;720:137296.
[35] Gabbe CJ, Mallen E, Varni A. Housing and urban heat: Assessing risk disparities. Housing Policy Debate 2023;33(5):1078–99.
[36] Wüstemann H, Kalisch D, Kolbe J. Access to urban green space and environmental inequalities in Germany. Landsc Urban Plan 2017;164:124–31.
[37] Csomós G, Farkas JZ, Kovács Z. Access to urban green spaces and environmental inequality in post-socialist cities. Hungarian Geographical Bulletin 2020;69(2): 191–207.
[38] Sun Y, et al. Literature review reveals a global access inequity to urban green spaces. Sustainability 2022;14(3):1062.

[39] Wu Y, et al. Heat-prone neighbourhood typologies of European cities with temperate climate. Sustain Cities Soc 2022;87:104174.
[40] Viinikka A, et al. Associations of neighbourhood-level socioeconomic status, accessibility, and quality of green spaces in Finnish urban regions. Appl Geogr 2023;157:102973.
[41] European Environment Agency. Who benefits from nature in cities? Social inequalities in access to urban green and blue spaces across Europe. 2022.
[42] Konijnendijk C. The 3–30-300 rule for urban forestry and greener cities. Biophilic Cities J 2021;4(2):2.
[43] Konijnendijk CC. Evidence-based guidelines for greener, healthier, more resilient neighbourhoods: Introducing the 3–30–300 rule. J For Res 2023;34(3):821–30.
[44] Przewoźna P, et al. Accessibility to urban green spaces: A critical review of WHO recommendations in the light of tree-covered areas assessment. Ecol Indic 2024;166:112548.
[45] Cadot E, Rodwin VG, Spira A. In the heat of the summer: lessons from the heat waves in Paris. J Urban Health 2007;84:466–8.
[46] Fouillet A, et al. Excess mortality related to the August 2003 heat wave in France. Int Arch Occup Environ Health 2006;80:16–24.
[47] Gabbe CJ, Gregory Pierce. The Roles of Housing and Household Characteristics in U.S. Residential Heat Risk. Findings 2024. https://doi.org/10.32866/001c.116607.
[48] Murage P, et al. What individual and neighbourhood-level factors increase the risk of heat-related mortality? A case-crossover study of over 185,000 deaths in London using high-resolution climate datasets. Environ Int 2020;134:105292.
[49] Park G-R. Health Inequalities in Housing: Housing Cost Burden, Housing Assets, and Mortality. 2023.
[50] Park G-R. Housing cost burden and external causes of mortality: Variations across housing regimes in high-income countries, 2010–2020. Soc Sci Med 2024;345:116672.
[51] Park G-R, et al. The association between housing cost burden and avoidable mortality in wealthy countries: cross-national analysis of social and housing policies, 2000–2017. J Epidemiol Community Health 2023;77(2):65–73.
[52] Tavares AI, Costa E, Albuquerque P. Housing cost overburden and population health: cross-country evidence from Europe before the pandemic. Int Rev Appl Econ 2024:1–17.
[53] Sandholz S, et al. Rethinking urban heat stress: Assessing risk and adaptation options across socioeconomic groups in Bonn. Germany Urban Climate 2021;37:100857.
[54] Uejio CK, et al. Intra-urban societal vulnerability to extreme heat: the role of heat exposure and the built environment, socioeconomics, and neighbourhood stability. Health Place 2011;17(2):498–507.
[55] Hsu A, et al. Disproportionate exposure to urban heat island intensity across major US cities. Nat Commun 2021;12(1):2721.
[56] Kim J, Ewing R, Rigolon A. *Does green infrastructure affect housing prices* via *extreme heat and air pollution mitigation? A focus on green and climate gentrification in Los Angeles County, 2000–2021*. Sustain Cities Soc 2024;102:105225.
[57] Cai Z, et al. Assessing the heat vulnerability of different local climate zones in the old areas of a chinese megacity. Sustainability 2019;11(7):2032.
[58] Kang Y, et al. Feeling the heat: extreme temperatures and housing prices in China. J Econ Surv 2024;38(5):1956–82.
[59] Deng H, et al. Household income inequality aggravates high-temperature exposure inequality in urban China. J Environ Manag 2020;275:111224.
[60] Chen F, Zhang J, Chen Z. Heat waves and housing markets: assessing the effects on real estate prices in China. Environ Resour Econ 2025;88(6):1541–79.
[61] Fernandez Perez A, Puig M Gómez, Rivero SJ Sosvilla. Hot Property: A Spatial Analysis of Temperature and Housing Prices in Spain. 2025.
[62] Cascarano M, Natoli F. Temperatures and search: evidence from the housing market. Bank of Italy Temi di Discussione (Working Paper) 2023:1419.
[63] Giraldo C, et al. Climate Hazards Meet Overpriced Cities: Linking Environmental Risks to Real Estate Markets Across the Globe. 2025.
[64] Pascal M, et al. Analysing effect modifiers of the temperature-mortality relationship in the Paris region to identify social and environmental levers for more effective adaptation to heat. Health Place 2024;89:103325.
[65] Sestito B, et al. Identifying vulnerability factors associated with heatwave mortality: a spatial statistical analysis across Europe. Environ Res Lett 2025;20(4):044025.
[66] Ichim P, et al. Characteristics of nocturnal urban heat island of Iaşi During a summer heat wave (1–6 of August 2017). Aerul si Apa. Componente ale Mediului 2018:253–60.
[67] Gherasim MP, et al. Gis analyzes on the urban heat island and newly built areas the city of iasi. In: International Multidisciplinary Scientific Geoconference: SGEM. 22; 2022. p. 287–94. 4.2.
[68] Sfîcă L, et al. Surface urban heat island of Iași city (Romania) and its differences from in situ screen-level air temperature measurements. Sustain Cities Soc 2023;94:104568.
[69] Hoffmann K, et al. Klimauntersuchungen in Jena für die Anpassung an den Klimawandel und seine erwarteten Folgen: Ein Ergebnisbericht. 2014.
[70] Kıvılcım B, Bradley PE. A data-driven approach for urban heat island predictions: rethinking the evaluation metrics and data preprocessing. Urban Sci 2025;9(5):151.
[71] Kurmutz U. Analyse der lokalen Auswirkungen des Klimawandels und Ableitung von Planungshinweisen für die Klimaanpassung am Beispiel der Stadt Jena. *https://nbn-resolving.org/urn:nbn:de:gbv:27-dbt-20,170,712-1,447,123*; 2017.
[72] Hjort J, Suomi J, Käyhkö J. Extreme urban–rural temperatures in the coastal city of Turku, Finland: Quantification and visualization based on a generalized additive model. Sci Total Environ 2016;569:507–17.
[73] Suomi J. Characteristics of urban heat island (UHI) in a high latitude coastal city-a case study of Turku. SW Finland. 2014.
[74] Ruosteenoja K, Jylhä K. Heatwave projections for Finland at different levels of global warming derived from CMIP6 simulations. Geophysica 2023;58(1).
[75] Suomi J, et al. Evaluation of surface air temperature in the HARMONIE-AROME weather model during a heatwave in the coastal city of Turku. Finland Urban Climate 2024;53:101811.
[76] Wu X, et al. Future heat-related mortality in Europe driven by compound day-night heatwaves and demographic shifts. Nat Commun 2025;16(1):7420.
[77] Ruuhela R, et al. Temperature-related mortality in Helsinki compared to its surrounding region over two decades, with special emphasis on intensive heatwaves. Atmosphere 2020;12(1):46.
[78] Kollanus V, Tiittanen P, Lanki T. Mortality risk related to heatwaves in Finland – factors affecting vulnerability. Environ Res 2021;201:111503.
[79] Näyhä S. Heat mortality in Finland in the 2000s. Int J Circump Health 2007;66(5):418–24.
[80] Landreau A, et al. Combining socio-economic and climate projections to assess heat risk. Clim Chang 2021;167(1):12.
[81] Päivärinne V, et al. Socioeconomic disparities in heat vulnerability among adults in Finland. Sci Rep 2025;15(1):20611.
[82] Farahani AV, et al. Hot summers in nordic apartments: exploring the correlation between outdoor weather conditions and indoor temperature. Buildings 2024;14(4):1053.
[83] Sohail H, et al. Heat, heatwaves and cardiorespiratory hospital admissions in Helsinki, Finland. Int J Environ Res Public Health 2020;17(21):7892.
[84] Ruuhela R, et al. Biometeorological assessment of mortality related to extreme temperatures in Helsinki Region, Finland, 1972–2014. Int J Environ Res Public Health 2017;14(8):944.
[85] Sfîcă L, Ichim P, Amihăesei V-A, Hrițac R, Irașoc A, Crețu C-Ș, et al. UCLARIS – urban thermo-hygrometric gridded dataset for Iasi city, Romania (Version 1) [Data set]. Zenodo 2023;2023.
[86] Eurostat - Income and living conditions. 2025.
[87] Ana Martinez; Pietro Florio; Cristiano Giovando; Katarzyna Goch (2026): DBSM R2023 - Individual building footprints for EU27 from the hierarchical conflation of OSM, Microsoft Buildings and ESM R2020. European Commission, Joint Research Centre [Dataset] doi: 10.2905/JRC.24QRN70 PID: http://data.europa.eu/89h/60c6b14d-3dda-4034-b461-390dc8ed8665.
[88] Copernicus (EEA). Urban Atlas Building Height 2012 (raster 10 m), Europe version 3. 2022.
[89] European Union's Copernicus Land Monitoring Service - Tree Cover Density 2018 - Present (raster 100 m), Europe. 2024. https://doi.org/10.2909/4dc35722-09ce-427f-9a1b-775a8640da27.2021.
[90] European Union's Copernicus Land Monitoring Service - Share of Built-Up 2018 (raster 100 m), Europe, 3-yearly. 2020. https://doi.org/10.2909/a807e528-431a-4dca-a6cd-0e8947563fce.2018.
[91] European Union's Copernicus Land Monitoring Service - Grassland 2017 - Present (raster 100m), Europe. 2024. https://doi.org/10.2909/5453c92f-3d01-4407-99bc-4659cfc7661d.
[92] European Union's Copernicus Land Monitoring Service - Urban Atlas Land Cover/Land Use 2018 (vector), Europe, 6-yearly. 2021.
[93] Cardona OD, van Aalst MK, Birkmann J, Fordham M, McGregor G, Perez R, et al. Determinants of risk: exposure and vulnerability. In: Managing the Risks of Extreme Events and Disasters to Advance Climate Change Adaptation. In: Field CB, Barros V, Stocker TF, Qin D, Dokken DJ, Ebi KL, Mastrandrea MD, Mach KJ, Plattner G-K, Allen SK, Tignor M, Midgley PM, editors. A Special Report of Working Groups I and II of the Intergovernmental Panel on Climate Change (IPCC). Cambridge, UK, and New York, NY, USA:: Cambridge University Press; 2012. p. 65–108.
[94] Cresswell K. A Florida urban heat risk index: Assessing weighting and aggregation approaches. Urban Clim 2023;51:101646.
[95] Morabito M, et al. Urban-hazard risk analysis: Mapping of heat-related risks in the elderly in major Italian cities. PLoS One 2015;10(5):e0127277.
[96] Xiang Y, et al. Heat risk assessment and response to green infrastructure based on local climate zones. Build Environ 2024;248:111040.
[97] Rausand M. Risk Assessment: Theory, Methods, and Applications115. John Wiley & Sons; 2013.
[98] Lauwaet D, et al. High resolution modeling of the urban heat island of 100 European cities. Urban Clim 2024;54:101850.
[99] Breitner S, et al. Short-term effects of air temperature on mortality and effect modification by air pollution in three cities of Bavaria, Germany: a time-series analysis. Sci Total Environ 2014;485–486:49–61.
[100] Ruuhela R, Hyvärinen O, Jylhä K. Regional assessment of temperature-related mortality in Finland. Int J Environ Res Public Health 2018;15(3):406.
[101] Cheval S, et al. A country scale assessment of the heat hazard-risk in urban areas. Build Environ 2023;229:109892.
[102] Finnish Meteorological Institute: Warnings for hot and cold weather. Available from: https://en.ilmatieteenlaitos.fi/warnings-on-hot-and-cold-weather; 2025.
[103] Robert Koch Institut (RKI): Hitzebedingte Mortalität in Deutschland. *2022*.
[104] Huber V, et al. Heat-related mortality in the extreme summer of 2022. Dtsch Arztebl Int 2024;121(3):79–85.
[105] Lwin K, Murayama Y. A GIS approach to estimation of building population for micro-spatial analysis. Trans GIS 2009;13(4):401–14.
[106] Ma L, et al. Investigating urban heat-related health risks based on local climate zones: a case study of Changzhou in China. Sustain Cities Soc 2023;91:104402.
[107] Brenning, A., Henn, S., 2023. Web scraping: a promising tool for geographic data acquisition. arXiv preprint arXiv:2305.19893. https://arxiv.org/abs/2305.19893.

[108] Brown MA, et al. Web scraping for research: legal, ethical, institutional, and scientific considerations. Big Data & Society 2025;12(4):20539517251381686.
[109] Krotov V, Johnson L, Silva L. Tutorial: Legality and ethics of web scraping. 2020.
[110] Logos K, et al. Establishing a framework for the ethical and legal use of web scrapers by cybercrime and cybersecurity researchers: learnings from a systematic review of Australian research. Int J Law Inform Technol 2023;31(3):186–212.
[111] Hengl T, Heuvelink GB, Stein A. Comparison of kriging with external drift and regression-kriging. 2003.
[112] Burrough P. GIS and geostatistics: Essential partners for spatial analysis. Environ Ecol Stat 2001;8:361–77.
[113] OpenStreetMap contibutors, Map data copyrighted OpenStreetMap contributors. *and available from*, *https://www.openstreetmap.org*.
[114] Banerji A, et al. House price developments in Europe: A comparison. International Monetary Fund; 2008.
[115] Czembrowski P, Kronenberg J. Hedonic pricing and different urban green space types and sizes: insights into the discussion on valuing ecosystem services. Landsc Urban Plan 2016;146:11–9.
[116] Kim H-S, et al. Understanding the local impact of urban park plans and park typology on housing price: a case study of the Busan metropolitan region. Korea Landscape and Urban Planning 2019;184:1–11.
[117] Lutzenhiser M, Netusil NR. The effect of open spaces on a home's sale price. Contemp Econ Policy 2001;19(3):291–8.
[118] Melichar J, Kaprová K. Revealing preferences of Prague's homebuyers toward greenery amenities: the empirical evidence of distance–size effect. Landsc Urban Plan 2013;109(1):56–66.
[119] Buiga A, Popa M. Determinants of rent prices: an analysis of European Cities. Studia Universitatis Babes-Bolyai 2025;70(1):51–66.
[120] Heyman AV, Sommervoll DE. House prices and relative location. Cities 2019;95: 102373.
[121] Lavell A, et al. Climate change: new dimensions in disaster risk, exposure, vulnerability, and resilience. In: Managing the risks of extreme events and disasters to advance climate change adaptation: Special report of the intergovernmental panel on climate change. Cambridge University Press; 2012. p. 25–64.
[122] Sakka A, et al. On the thermal performance of low income housing during heat waves. Energ Buildings 2012;49:69–77.
[123] Dewilde C, Lancee B. Income inequality and access to housing in Europe. Eur Sociol Rev 2013;29(6):1189–200.
[124] Santamouris M, Kolokotsa D. On the impact of urban overheating and extreme climatic conditions on housing, energy, comfort and environmental quality of vulnerable population in Europe. Energ Buildings 2015;98:125–33.
[125] Witte N. Visualizing the housing cost burden of migrants and natives across the income distribution. Socius 2024;10:23780231241298806.
[126] Filandri M, Pasqua S, Tucci V. Housing tenure and subjective poverty among young European adults: The role of rent regulation. Journal of European Social Policy 2025;35(4):332–48.
[127] Chakraborty T, et al. Disproportionately higher exposure to urban heat in lower-income neighbourhoods: a multi-city perspective. Environ Res Lett 2019;14(10): 105003.
[128] Browning M, et al. Measuring the 3–30-300 rule to help cities meet nature access thresholds. Sci Total Environ 2024;907:167739.
[129] Sützl BS, et al. Urban morphology clustering analysis to identify heat-prone neighbourhoods in cities. Sustain Cities Soc 2024;107:105360.
[130] Russo S, et al. Half a degree and rapid socioeconomic development matter for heatwave risk. Nat Commun 2019;10(1):136.
[131] Gao S, et al. Urbanization-induced warming amplifies population exposure to compound heatwaves but narrows exposure inequality between global North and South cities. Npj Climate and Atmospheric Science 2024;7(1):154.
[132] Chen B, et al. Diurnal heat exposure risk mapping and related governance zoning: a case study of Beijing. China Sustainable Cities and Society 2022;81:103831.
[133] Bhattarai S, et al. Spatiotemporal characterization of heatwave exposure across historically vulnerable communities. Sci Rep 2024;14(1):20882.
[134] Wrotek M, et al. From inequalities to vulnerability paradoxes: juxtaposing older adults' heat mortality risk and heat experiences. Environ Health 2025;24(1):24.
[135] de Schrijver E, et al. Exploring vulnerability to heat and cold across urban and rural populations in Switzerland. Environ Res Health 2023;1(2):025003.
[136] Dialesandro J, et al. Dimensions of thermal inequity: neighbourhood social demographics and urban heat in the southwestern U.S. Int J Environ Res Public Health 2021;18(3).
[137] Murage P, Hajat S, Kovats RS. Effect of night-time temperatures on cause and age-specific mortality in London. Environ Epidemiol 2017;1(2):e005.
[138] Berger T, et al. Low-income residents' strategies to cope with urban heat. Land Use Policy 2022;119:106192.
[139] Sfîcă L, et al. The extent and intensity of the urban heat island in Iași city. Romania Theoret Appl Climatol 2018;134(3):777–91.
[140] Kadhim-Abid AL, Ichim P, Atanasiu GM. Seasonal occurrence of heat island phenomenon in the urban built environment. Environ Eng Manag J (EEMJ) 2019; 18(2).
[141] Rippstein V, et al. Trends in tropical nights and their effects on mortality in Switzerland across 50 years. PLOS Climate 2023;2(4):e0000162.
[142] Błażejczyk K, et al. Heat strain and mortality effects of prolonged central European heat wave-an example of June 2019 in Poland. Int J Biometeorol 2022; 66(1):149–61.
[143] Ioannou LG, et al. Impact of a simulated multiday heatwave on nocturnal physiology, behavior, and sleep: a 10-day confinement study. Appl Physiol Nutr Metab 2024;49(10):1394–408.
[144] Nguyen JL, Schwartz J, Dockery DW. The relationship between indoor and outdoor temperature, apparent temperature, relative humidity, and absolute humidity. Indoor Air 2014;24(1):103–12.
[145] Zorn A, et al. Zugang zu urbanen Grünflächen im Kontext von Hitzeereignissen am Beispiel von Jena. Standort 2021;45(4):265–71.
[146] Tian Y, et al. Urban green inequality and its mismatches with human demand across neighbourhoods in New York, Amsterdam, and Beijing. Landsc Ecol 2024; 39(3):60.
[147] Rocha AD, et al. Unprivileged groups are less served by green cooling services in major European urban areas. Nature Cities 2024;1(6):424–35.
[148] McDonald R, et al. Planting healthy air: a global analysis of the role of urban trees in addressing particulate matter pollution and extreme heat. 2016.
[149] Shi Z, et al. Modeling the intensity of surface urban heat island based on the impervious surface area. Urban Clim 2023;49:101529.
[150] Li Y, et al. Green spaces provide substantial but unequal urban cooling globally. Nat Commun 2024;15(1):7108.
[151] Li H, et al. Cooling efficacy of trees across cities is determined by background climate, urban morphology, and tree trait. Commun Earth Environ 2024;5(1): 754.
[152] Locke DH, et al. Residential housing segregation and urban tree canopy in 37 US Cities. npj Urban Sustainability 2021;1(1):15.
[153] Nguyen JL, Dockery DW. Daily indoor-to-outdoor temperature and humidity relationships: a sample across seasons and diverse climatic regions. Int J Biometeorol 2016;60:221–9.
[154] Božič A. Relationship between indoor and outdoor temperature and humidity in a residential building in Central Europe. Discover Environment 2024;2(1):63.
[155] Chong D, Zhu N. Human heat acclimatization in extremely hot environments: a review. Procedia Eng 2017;205:248–53.
[156] McMichael AJ, et al. International study of temperature, heat and urban mortality: the 'ISOTHURM' project. Int J Epidemiol 2008;37(5):1121–31.
[157] Turrisi TB, et al. Seasons, weather, and device-measured movement behaviors: a scoping review from 2006 to 2020. Int J Behav Nutr Phys Act 2021;18:1–26.
[158] Leichtle T, et al. Quantifying urban heat exposure at fine scale-modeling outdoor and indoor temperatures using citizen science and VHR remote sensing. Urban Clim 2023;49:101522.
[159] Peerlings E, et al. Indoor heat in Amsterdam: comparing observed indoor air temperatures from a professional network and from a citizen science approach. City and Environment Interactions 2024;24:100173.
[160] Rajagopalan P, Andamon MM, Paolini R. Investigating thermal comfort and energy impact through microclimate monitoring-a citizen science approach. Energ Buildings 2020;229:110526.